Optical Fiber Technology **8**, 43–70 (2002)
doi:10.1006/ofte.2001.0371, available online at http://www.idealibrary.com on IDEAL®

Invited Paper

On Architecture and Limitation of Optical Multiprotocol Label Switching (MPLS) Networks Using Optical-Orthogonal-Code (OOC)/Wavelength Label

Y. G. Wen, Y. Zhang, and L. K. Chen

Department of Information Engineering, The Chinese University of Hong Kong, Shatin, New Territories, Hong Kong, Special Administrative Region, China
E-mail: yzhang0@ie.cuhk.edu.hk

Received October 22, 2001

To accommodate the explosive packet-based data traffic in WDM networks, intelligent optical routing and switching are required in optical transport networks. Optical multiprotocol label switching networks emerged to meet this demand. In this paper, different schemes for implementing an OMPLS network are introduced. An optical MPLS network using OOC/wavelengths as labels is proposed. Based on an all-optical code converter, the architecture of the optical core router is demonstrated. The fundamental limits on scalability of the proposed core router, namely the label capacity, and the blocking probability of the label switched path setup are investigated, and closed-form solutions are derived.

Key Words: optical multiprotocol label switching; optical orthogonal code; code/wavelength label; optical code conversion.

I. INTRODUCTION

To meet the mounting bandwidth requirement brought by Internet traffic, the emerging dense wavelength-division-multiplexing (DWDM) technology is essential. Proposed originally as a means to dramatically increase the transmission capacity in a single fiber, WDM network designs have evolved to provide other desirable features, including protocol transparency, dynamic reconfigurability, and improved survivability, outperforming the traditional SDH/SONET networks [1–5, 10].

1068-5200/02 $35.00

To accommodate packet-based data traffic in WDM networks, emerging WDM networks need to support intelligent optical routing and switching. For this purpose, efficient routing can be achieved by the collapse of the protocol stacks [6], which leads to the design of slim protocol stacks with flexible bandwidth-on-demand and dynamic reconfigurability features [7]. In these designs, the optical multiprotocol label switching (OMPLS) technique is employed to allow efficient packet forwarding while decoupling the packet routing and forwarding operations to support multiple-routing services [8]. In the future, MPLS will be used as a unifying network management and traffic engineering protocol for a variety of transport systems and would be extended to generalized multiprotocol label switching (GMPLS) [9].

As shown in Fig. 1a, traditional network designers incorporate several standard layers (IP over ATM over SONET/SDH over optical) to implement optical systems. Merging these layers can enhance WDM networks to provide protocol transparency, dynamic reconfigurability and improved survivability. In Fig. 1, two solutions based on multiprotocol label switching (MPLS) technology are proposed for collapsing protocol stacks. Figure 1b shows the one using the combination of IP and MPLS over the optical layer. The combination of IP and MPLS promises interoperability and end-to-end QoS, whereas the optical layer provides high-capacity transport, reliable transport, and bandwidth management. The other approach shown in Fig. 1c has MPLS in the optical layer and provides an OMPLS interface for upper layers, such as the IP layer. This scheme has great potential as it promises simplified forwarding and all-optical label swapping.

In this paper, for the second approach, an optical MPLS network using OOC/wavelengths as labels is proposed. Based on an all-optical code converter, we proposed an architecture for an optical core router. The fundamental limits on scalability of the proposed core router, including the label capacity, and the blocking probability of the label switched path (LSP) setup are investigated with close-form solutions derived.

The paper is organized as follows. Section 2 presents an overview of the optical MPLS network and optical label schemes. Section 3 provides the details of implementing the all-optical OMPLS core router. Section 4 presents the scalability of the photonic MPLS network with code/wavelength labels, whose performances should

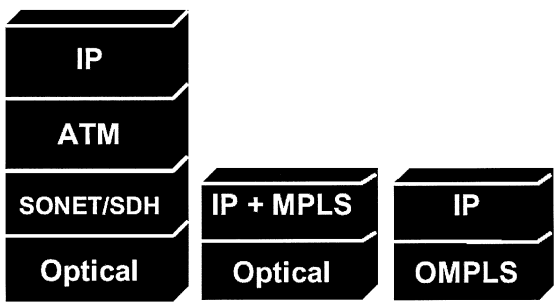

FIG. 1. Protocol stack solutions for transport of IP-over-WDM networks. (a) Traditional approach, (b) IP/MPLS approach, and (c) IP over OMPLS approach.

be determined by the implementation of the fabric and the deployment of conversion capability. Section 5 concludes this paper.

II. OPTICAL MPLS SCHEMES

A generic photonic MPLS network [11,12] is shown in Fig. 2. The source node A generates IP packets, which are routed by conventional electronic routers to an ingress router in the photonic MPLS network. Labels are added onto IP packets at the optical edge switch located at the ingress router. The optical core switches perform routing and forwarding by label swapping. When packets leave the photonic MPLS network at the egress router, the edge routers remove the labels and forward the packets to its destination.

Figure 2b depicts the physical layer network elements connected by fiber links and the packet routing and forwarding hierarchy [13]. IP packets are generated at the electronic routing layer (IP routers) and processed in an OMPLS adaptation layer that encapsulates IP packets with an optical label without modifying the original packet structure. The adaptation layer also converts the packet and label to a new wavelength specified by local routing tables. An optical multiplexing layer multiplexes labeled packets onto a shared fiber medium. Several optical multiplexing approaches may be used including insertion directly onto an available WDM channel [14], packet compression through optical time multiplexing or time interleaving through optical time division multiplexing [15], and optical code-division multiplexing [4]. In the optical MPLS network, core routers, which can be partitioned into two basic parts: control component and forwarding component, perform routing and forwarding functions. In the control component, the routing algorithm computes a new label and wavelength from an internal routing table giving the current label and optical interface (including current wavelength and fiber port). The routing tables (at egress and core routers) are generated by mapping IP addresses into smaller pairs of labels and wavelengths and distributing them across the network via piggyback on top of routing protocols (e.g., OSPF or PIM) or a separate protocol (e.g., Label Distribution Protocol) [16]. The forwarding component has the responsibility of swapping the original label with the new label and physically converting the labeled packet to the new wavelength. The reverse process of optical demultiplexing, adaptation and electronic routing are performed at the egress node.

As shown in Fig. 3, the label embedded in the IP packet could be carried by (a) time slot, (b) wavelength, (c) subcarrier, or (d) code and usually denotes critical label-switched-path information such as the source and destination. For optimum performance:

1. Optical labels should not consume wavelength resources originally dedicated for data channels;
2. Optical label swapping should be easily implemented, preferably in the optical domain;
3. Optical labels should be immune to accumulated distortions from dispersion, timing jitter, and interference from other co-propagation labels.

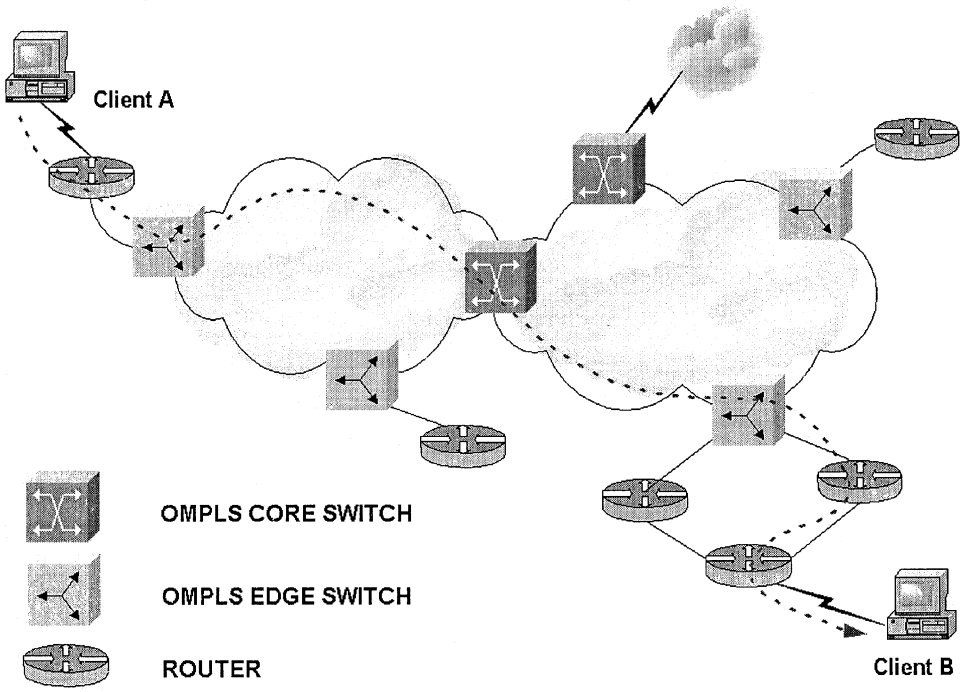

(a)

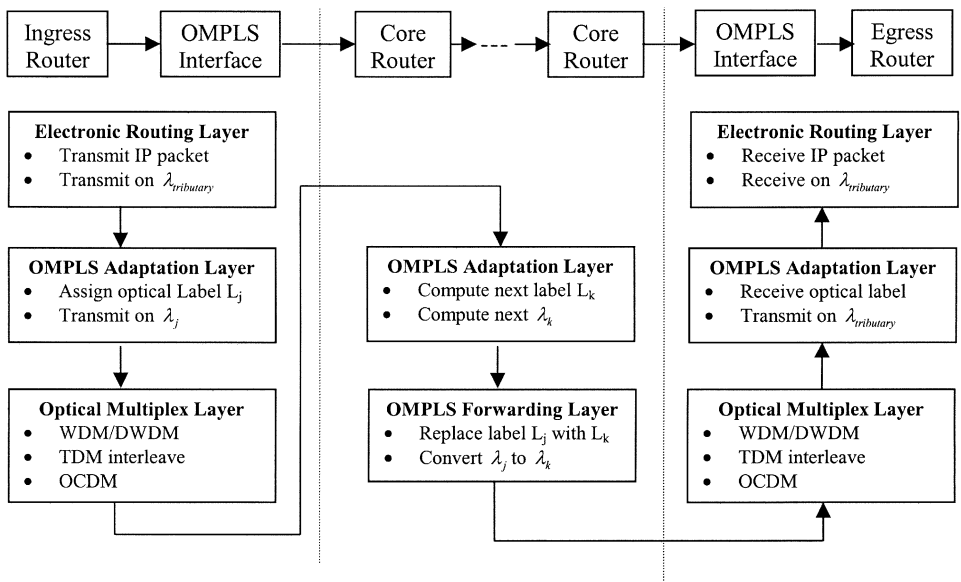

(b)

FIG. 2. (a) A generic optical multiprotocol label switching (OMPLS) network. The dashed line shows the label switched path (LSP) that routes data from the source, through the router, edge switch, and core switch, to the destination. (b) Layered routing and forwarding hierarchy and associated network element connection diagram for a generic OMPLS network.

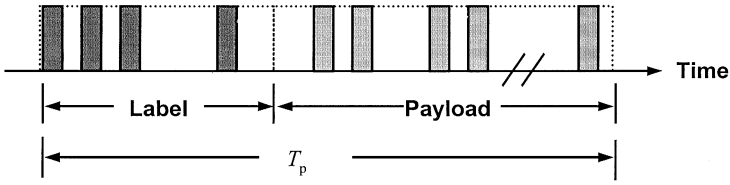

3(a) Time-Division Label Scheme

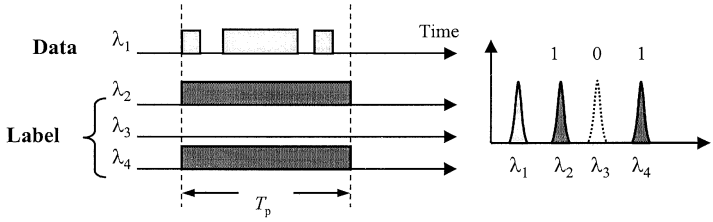

3(b) Wavelength-Division Label Scheme

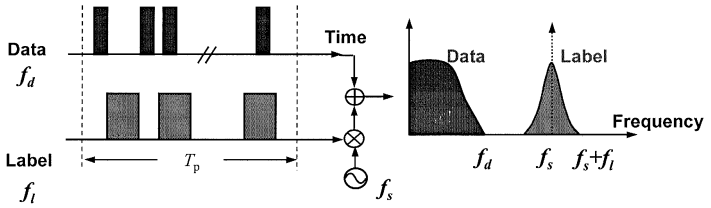

3(c) Frequency-Division Label Scheme

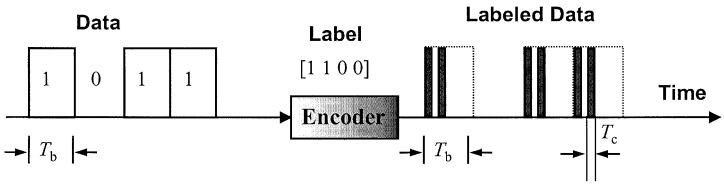

3(d) Code-Division Label Scheme

FIG. 3. The schemes of optical label technologies: (a) time-domain overhead label, (b) subcarrier label, (c) time-spreading code label, and (d) wavelength-spreading code label. T_p is the packet duration; f_d and f_l are the rates of the data and the label; f_s is the subcarrier frequency; T_b and T_c are the durations of the data bit and the code chip; λ_1 is the carrier of data; $[\lambda_2, \lambda_3, \lambda_4]$ are for the label; different combinations of these carriers denote different labels.

Based on these criteria, four primary OMPLS schemes have been proposed previously. As shown in Fig. 3, there are (1) a time-division label scheme, (2) a wavelength-division label scheme, (3) a frequency-division label scheme, and (4) a code-division label scheme.

1. Time-Division OMPLS Scheme

Figure 3a shows a schematic diagram of the time-division OMPLS scheme. In this label scheme, optical labels are implemented by adding a routing header before the payload in the time domain. The bit rate of the routing header is usually the same as or lower than the data rate [5]. The former avoids much buffering time

for label processing, but puts some challenges on the processing capacity of the label processor. Since the label rate is the same as the data rate, for the current transport networks, the label processor must work at a multi-Gbps rate to process label recovery, label swapping, and packet forwarding. The latter processes labels at a comparably lower rate, but needs more buffering time for the fixed number of optical label bits. Due to the mature electronics technologies (e.g., FPGA and ASIC) in a lower processing rate, this approach is preferable at current stage.

All-optical label processing (recovery, swapping, and reinserting) is essentially important for OMPLS networks. For the time-division label scheme, a traditional header processor could be introduced for label processing. However, with the coherent nature of optical routing labels, label swapping can be realized by optical label conversion with a simple XOR gate [17]. Its operation principle is simple, just using another sequence (swapping sequence) to change the old label via optical XOR processing.

2. Wavelength-Division OMPLS Scheme

A wavelength-division optical label is also called a wavelength-coded label. Shown in Fig. 3b, three public wavelengths (λ_2, λ_3, and λ_4) are reserved for label coding, and the data payload is carried only on the lightwave carrier (λ_1). Different combinations of presence or absence of these three public wavelengths, represent different destination labels. In Fig. 3b, λ_2 and λ_4 are present and λ_3 is absent; thus the coded wavelength label is [1 0 1]. For an N-public-wavelength label system, the total number of wavelength labels is (2^N). Therefore, though only N wavelengths are reserved for label coding, this number is small compared with the supportable data channels (2^N). This is a large improvement compared with that of a multiprotocol lambda label switching network.

For a wavelength-division OMPLS network, the all-optical label switching router (core router) is easier to implement than other OMPLS schemes, since it can be implemented with a fiber Bragg grating (FBG). One representative system based on wavelength-division OMPLS networks was proposed by Wada and Harai [18], though their proposal has very low wavelength efficiency. As shown in Fig. 4, the header carries a wavelength-coded label that corresponds to a destination node. In the scheme, multiwavelength labels are carried on λ_{1A}, λ_{1B}, λ_{1C}, and λ_{1D}. Payload data use another different wavelength (λ_{1E}). Wavelengths ranging from λ_{1A} through λ_{1E} are defined as a wavelength band λ_{1A-E}.

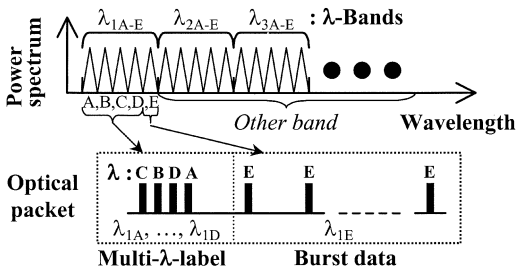

FIG. 4. Schematic diagram of packet format for multi-wavelength label switching scheme (from Ref. [18]).

3. Frequency-Division OMPLS Scheme

Figure 3c shows the operational principle of the frequency-division optical label scheme. In this scheme, the optical label is carried by an out-of-band subcarrier [6]. The payload and label are transmitted at different rates, and label recovery is performed independent of the payload data rate using simple microwave filtering techniques. Subcarrier label recovery is performed using optical and microwave amplitude detection, alleviating the need for RF coherent techniques and phase synchronization across the network. Furthermore, the mature electronics guarantees the practicability of the optical subcarrier label scheme. Thus, increasing attention is being paid to this type of label implementation and testbed [19–21].

Another attraction of frequency-division optical labels is packet transparency. In this scheme, packet transparency is realized by setting a fixed label bit rate and modulation format independent of the packet bit rate. The choice of label bit rate is determined by various factors including the speed of the burst-mode label recovery electronics and the duration of the label relative to the shortest packets at the fastest packet bit rates. Additionally, running the label at a lower bit rate allows the use of lower cost electronics to process the label. The label and packet bits can be encoded using different data formats to facilitate data and clock recovery.

On the other hand, a subcarrier label system limits the payload bit rate. In order to avoid the label's interference with the payload, there must be some guard-band between the payload spectrum and subcarrier spectrum.

Optical subcarrier label is the most promising candidate for OMPLS networks and all-optical label swapping using this scheme is gaining much attention in both academic and commercial institutes. Currently, researchers prefer using remove-and-reinsert mode label swapping for subcarrier label schemes. Basically, this is a three-stage label processing. At the first stage, the subcarrier label is extracted and removed in all-optical ways. At the second stage, the label is recovered and label information is fed to the control plane to determine the next label. In the final stage, the new label is remodulated at the same microwave carrier frequency for the IP packets. Currently, there are three major research projects on this scheme [19–21]. The first project is implemented at the University of California at Santa Barbara (UCSB) [19]. The second experimental testbed is reported from the University of California at Davis [20]. The third testbed [21] was implemented as a joint project of National Chiao-Tung University and Telecordia Technologies.

4. Code-Division OMPLS Scheme

Recent progress in high-bit-rate optical code division multiplexing (OCDM) opens up a new way to use optical codes as optical labels [22]. This is a novel approach in that it eliminates any logic operation in the table look-up, which has been the toughest challenge for optical processing, and it only requires optical correlation [22].

In general, code-division optical encoding schemes are classified into coherent and noncoherent approaches according to the degree of coherence of the light source. Thus, there are also two alternative solutions for incorporating OCDM into code-division OMPLS schemes.

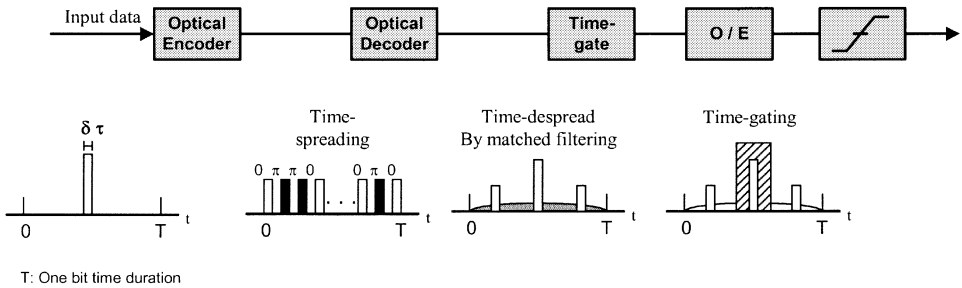

FIG. 5. Operation principle of coherent optical code division multiplexing (OCDM) (revised from Ref. [23]).

The first is the coherent approach proposed by Kitayama [23]. The operation principle of this approach is shown in Fig. 5.

For this proposal, label swapping can be implemented in an all-optical domain. A schematic diagram of photonic label swapping is shown in Fig. 6. Based on a cross phase modulation (XPM) effect, the operation principle is illustrated in Fig. 7. When the input signal pulse propagates along with the control optical pulse in an optical fiber, the refractive index seen by the input optical pulse is changed by the control pulse because of XPM. As a result, the input signal pulse experiences a phase shift $\Phi_{\max}$, which is determined by both the intensity of the control light and the interaction length. By appropriately setting the wavelength and intensity of the control pulse, the signal pulse will have a desired phase shift at the output of the fiber. For example, to swap the four-chip-long BPSK optical code, [0000] to a different code $[00\pi\pi]$, as shown in Fig. 7, the intensity of the control pulses have to be set so that the total phase shift becomes π. Therefore, all-optical label swapping is realized by using control pulses to change the phase of the signal pulses.

The noncoherent approach was proposed in Refs. [24, 25]. As shown in Fig. 3d, a data bit is modulated by an optical orthogonal code (OOC) in the time domain; that is, when the data bit is ONE, an OOC is sent out, and when the data bit is ZERO, no code is sent or the complementary format of the OOC is sent. This OOC also performs as the optical label, which can be used to forward the IP packet to its destination.

In Ref. [24], the sequence inversion keyed (SIK) direct spread (DS) code division multiple-access (CDMA) scheme is considered. In an optical SIK system, the data bits are modulated either by a unipolar signature sequence C_i or its complement $\overline{C_i}$, depending on whether the transmitting bit is ZERO or ONE, respectively. With this property, all-optical label swapping can be implemented by code conversion, which can be realized by processing the incoming code label and a control code with an optical XOR gate.

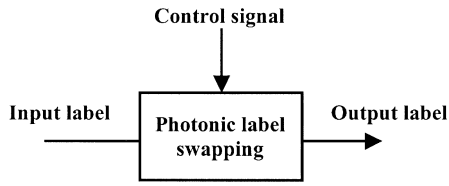

FIG. 6. Architecture of photonic label swapping for code-division label.

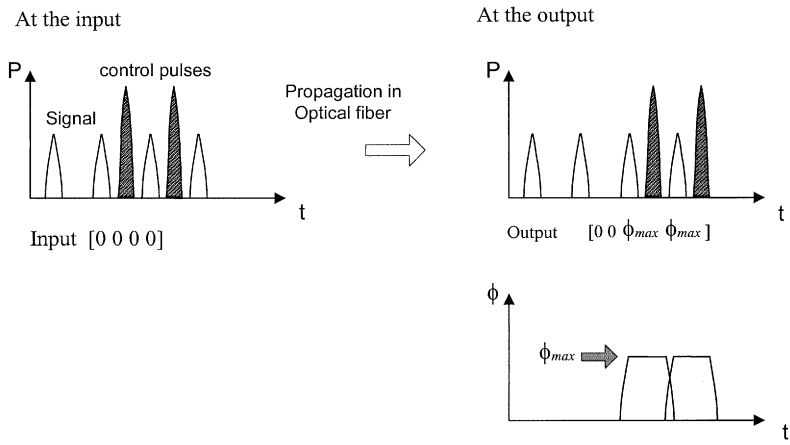

FIG. 7. Principle of photonic label swapping for code-division label (revised from Ref. [23]).

In the routing node, the input signal is a SIK DS-CDMA signal modulated by the code C_i, corresponding to the virtual optical code channel (VOCC) $VOCC(i)$. An optical code converter is used to convert the code C_i to code C_j, corresponding to the routing from $VOCC(i)$ to $VOCC(j)$. Here the concept of conversion code Q_{ij} is introduced. By processing the input signal with Q_{ij}, the information carried in the $VOCC(i)$ can be coupled to the $VOCC(j)$. Thus our proposed code converter realizes the all-optical CDMA switching function.

For the scheme, the conversion code Q_{ij} must have two properties of $C_i \oplus Q_{ij} = C_j$ and $\overline{C_i} \oplus Q_{ij} = \overline{C_j}$. It is found that with $Q_{ij} = C_i \oplus C_j$,

$$C_i \oplus Q_{ij} = C_i \oplus (C_i \oplus C_j) = C_i \oplus C_i \oplus C_j = 0 \oplus C_j = C_j$$
$$\overline{C_i} \oplus Q_{ij} = \overline{C_i} \oplus (C_i \oplus C_j) = \overline{C_i} \oplus C_i \oplus C_j = 1 \oplus C_j = \overline{C_j}.$$

Thus the unique conversion code $Q_{ij} = C_i \oplus C_j$, can facilitate the routing function from $VOCC(i)$ to $VOCC(j)$. For example, for the 4-chip Walsh codes having $C_1 = [1\ 0\ 1\ 0]$ and $C_2 = [1100]$, the code conversion function from C_1 to C_2 is verified by

$$Q_{12} = C_1 \oplus C_2 = [0\ 1\ 1\ 0]$$
$$C_1 \oplus Q_{12} = [1\ 0\ 1\ 0] \oplus [0\ 1\ 1\ 0] = [1\ 1\ 0\ 0] = C_2$$
$$\overline{C_1} \oplus Q_{12} = [0\ 1\ 0\ 1] \oplus [0\ 1\ 1\ 0] = [0\ 0\ 1\ 1] = \overline{C_2}.$$

Based on this principle, a proposed code converter is shown in Fig. 8. The code converter is a modified TOAD (terahertz optical asymmetric demultiplexer) that has two arms of control pulse input [36]. One is the routing node's input channel code C_i, and the other is the conversion code Q_{ij}. These two signals are of the same wavelength, whereas the XOR clock is on a different wavelength, such that they can be separated by an optical filter at the output port. After the clock enters the loop through the main coupler, it splits into two pulses, a clockwise (CW) and a counterclockwise (CCW) pulse. Each of these two pulses passes through the SOA (semiconductor optical amplifier) once, and returns to the main coupler at the same

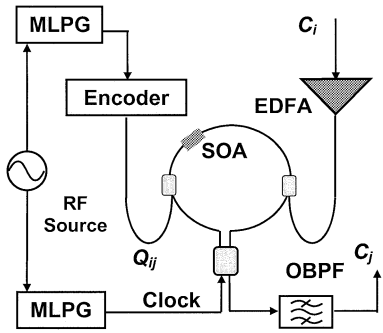

FIG. 8. A proposed code converter for OCDM OMPLS network. MPLG. mode-locked pulse generator. OBPF: optical bandpass filter.

time. When the two control arms have the same signal level, 1 or 0, the CW and CCW pulses will experience the same transmission properties of the SOA. The clock train is then totally reflected into the input port and no pulse appears in the output port. On the other hand, if one of the two control arms has a 1 level and the other has a 0 level, the CW and CCW pulses will experience different transmission properties of the SOA. The clock pulse train will come out from the output port of the TOAD when the phase difference between the CW and CCW pulses is π. Thus, the output channel code $C_j = C_i \oplus Q_{ij}$ is obtained at the output port of the code converter.

Another alternative code converter based on the same principle is shown in Fig. 9. The device is based on the XOR operation using a symmetric Mach–Zehnder interferometer [38].

However, none of these reported code-converted approaches investigates the fundamental issue of multiaccess interference (MAI), the cross-correlation between the selected code channel and the other co-propagation code channels. Thus, in Ref. [25], we proposed a switch fabric for an OOC MPLS core router, which take the MAI into consideration. In this paper, we would like to investigate and discuss in detail the architecture and scalability of an OOC-based MPLS core router. It should be noted that, in our proposed OMPLS scheme, the optical label actually is extended into two dimensions that are denoted by the combination of an OOC code and a wavelength in order to provide a larger label pool.

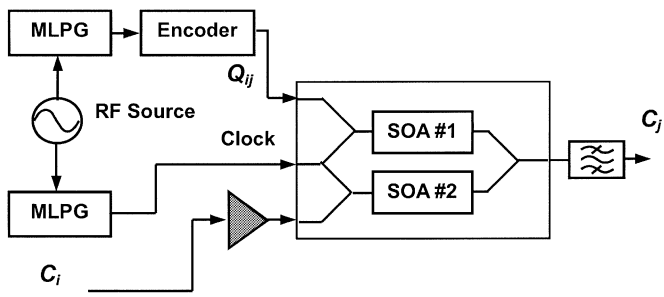

FIG. 9. Code converter using SMZ for OCDM OMPLS network.

III. ARCHITECTURE OF OOC/WAVELENGTH LABELED OMPLS NETWORK

1. Infrastructure of the Label Switch Router

As mentioned in Section II, several optical MPLS schemes were proposed previously, such as time-division [17], wavelength-division [18], frequency-division [19–21], and code-division [22–25] label schemes. In particular, the code-division label scheme has the advantages of employing optical orthogonal code (OOC) as labels and label swapping by code conversion. Thus, it alleviates the interference from other labels and noises due to the orthogonality of the optical code.

There are two approaches to using a code-division label, that is, coherent schemes (bipolar code and phase modulation) and noncoherent schemes (OOC code and intensity modulation). So far, for these approaches, all reported code conversion schemes can be classified into three different approaches. The first [26] is based on a coherent method, albeit its application is limited by fiber dispersion and polarization disturbance. The second relies on a look-up table and requires extensive, undesirable OE–EO processing [27]. The third scheme uses an all-optical logic XOR gate to implement the code converter [24]. Nevertheless, none of these reported code-converters considers the fundamental issue of multiaccess interference (MAI), the cross-correlation between the selected code channel and other co-propagation channels.

Due to the intrinsic unipolar property of the OOC set, MAI cannot be eliminated and will degrade the performance of packet switching networks. Thus, in this section, a MAI-suppression multichannel code converter will be presented, and the detrimental effects of MAI will be investigated.

Figure 10 shows a generic optical switch fabric for the MAI-suppression multichannel code conversion. The received optical signals in a single input fiber are composite signals consisting of code/wavelength channels (c, λ), with each channel uniquely described by a particular wavelength λ_i, $i = 1, 2, \ldots, N$, and a particular OOC c_i, $i = 1, 2, \ldots, M$, at any given time. The composite signals are first separated in the wavelength domain by an optical wavelength demultiplexer, for instance, an array waveguide grating (AWG). Following the AWG, the M code channels in each of the demultiplexed wavelengths are decorrelated by M decoders, each of which functions as a dedicate correlator. The output from each decoder will feed into a time-gate-intensity-threshold (TGIT) device. The TGIT device is necessary in order to differentiate the auto-correlation peaks from its subpeaks and cross-correlation peaks, all generated from the decorrelated optical pulse train. Accordingly, for a received data of ONE/ZERO bit, the corresponding autocorrelation peak is an optical pulse/null. It should also be noted that the TGIT device could be configured to perform wavelength conversion, thus offering an additional function of data routing.

Following the threshold device array is an optical space switch, which can be a nonblocking switch, such as a three-stage Clos network switch (Fig. 11), responsible for routing the optical pulses to different output ports. For channel add–drop, the channel is routed to a drop port. A new data channel is inserted through the add port of the optical space switch. For optical signal forwarding function, the optical pulse decoded from code channel i is routed to the input of the encoder of code

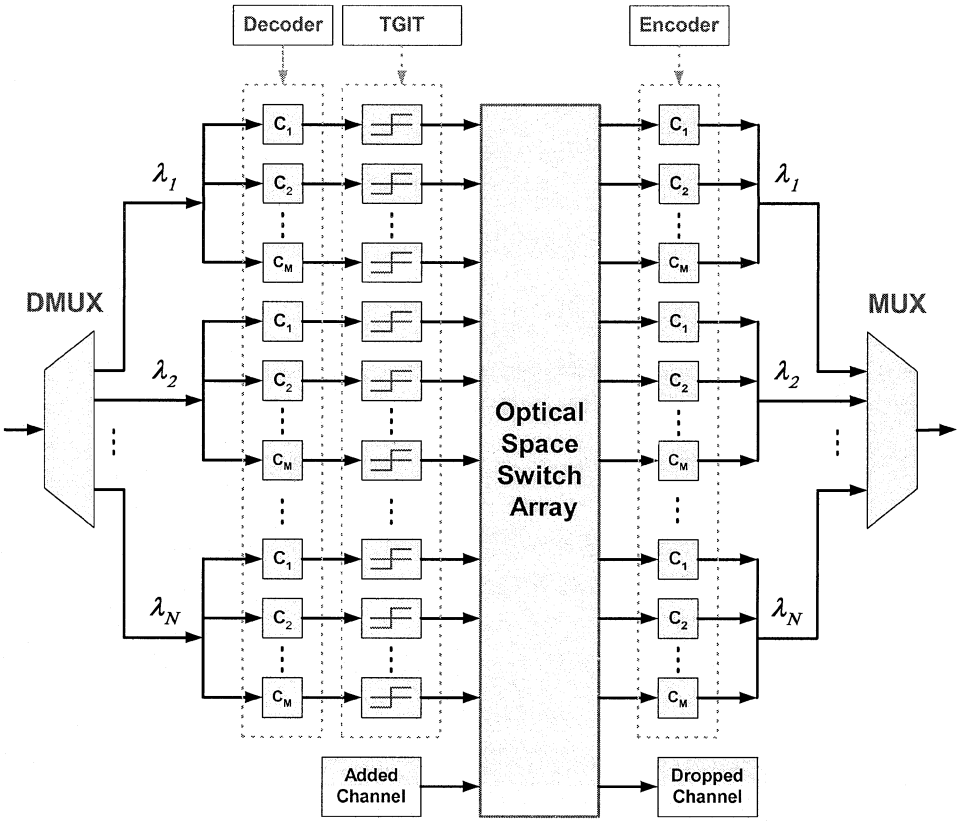

FIG. 10. The schematic diagram of the proposed core router fabric using code/wavelength label. TGIT: time-gating-intensity-thresholding device.

channel j designated for code j. Finally, the outputs of the encoder array are multiplexed by an AWG multiplexer into the output fiber and forwarded to the next switching node.

In general the optical MPLS core router would have multiple interfaces that support multifibers. Our proposed OMPLS core router can be extended to the multifiber case, and the schematic diagram is shown in Fig. 19.

2. Implementation of the Optical Label Swapping

In this part, the primary elements that implement the code/wavelength label swapping are investigated. These include the encoder, the decoder, and the threshold device.

A. Encoders/Decoders. For systems with an optical code-division label, the coding architecture of optical encoders/decoders is a very important factor. For example, power loss in encoders/decoders will impose restrictions on the power budget, the length of sequences, and the number of subscribers; the length of delays imposes restrictions on the size and cost of such a system. Therefore, much attention [28–30]

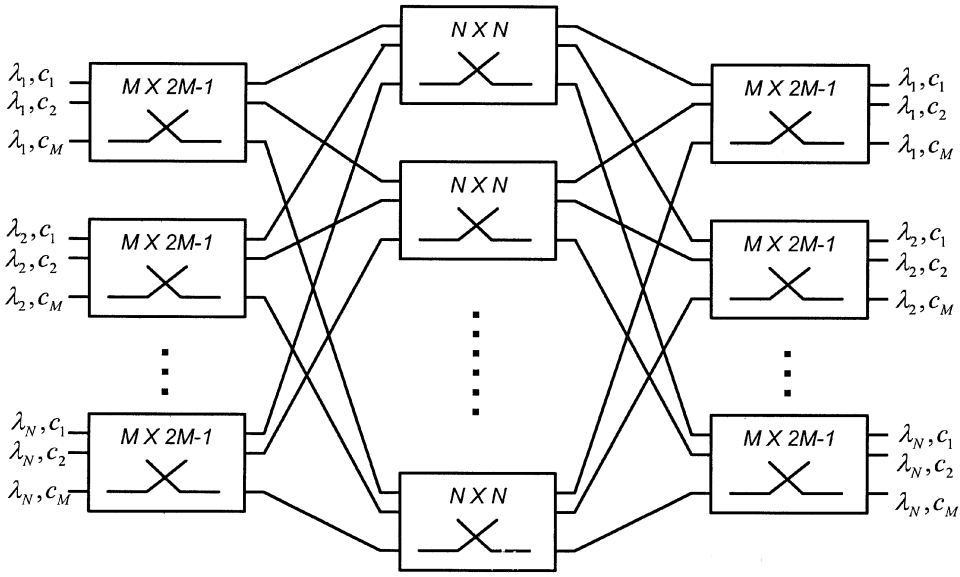

FIG. 11. The streamlined diagram of a three-stage Clos network for optical space switch.

has been paid to the design of good coding architectures to facilitate the implementation of an OCDM system.

In general, OOC encoders/decoders proposed previously can be classified into three categories: (1) all-parallel approach [31], (2) all-serial approach [32], and (3) serial-to-parallel approach.

All-parallel encoders/decoders. When OCDM was first proposed, an all-parallel encoder/decoder (Fig. 12) was commonly adopted in this research field. Its operation principle is very simple. At the first stage, the pulse source is split into N copies by the optical splitter. At the second stage, every individual copy of the pulse source passes through an optical delay line of various lengths with a step size τ from the 1st path to the Nth path. Then at the third stage, an electrical address signal is used to control the optical switch array that passes those optical signals corresponding

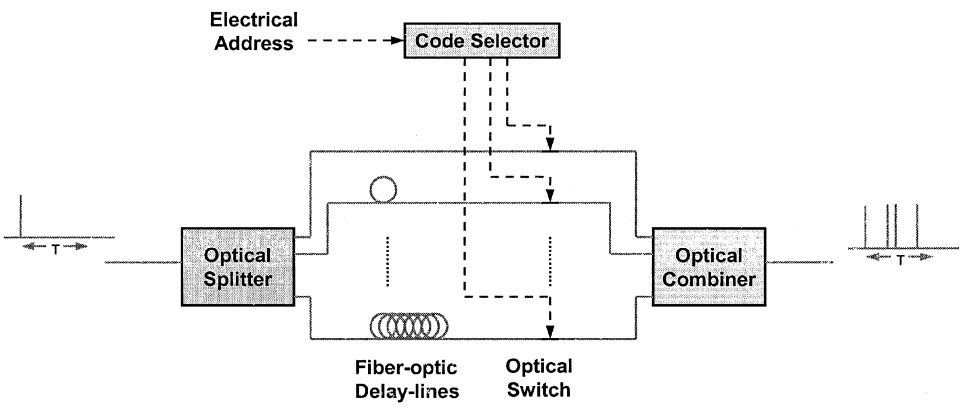

FIG. 12. All-parallel encoder.

to code bit ONE or cuts off those optical signals corresponding to code bit ZERO. Finally, at the fourth stage, the optical combiner combines all the optical signals to complete the coding processing. For the decoder, the same structure can be used similarly.

The implementation is desirable as it is a basic architecture for OOC encoders/decoders, with less implementation complexity. Though it originally was proposed for prime codes, it is suitable for any OOC family. However, it needs a large number of delay lines and switches. Moreover, it can only be used to encode a fixed length OOC.

All-serial encoders/decoders. Recent research on the use of fiber-optic lattice signal processing provided a better coding architecture for optical CDMA. Figure 13 shows the block diagram of the modified 2^n encoder, where an all-serial architecture is used for code sequence generation, selection, and correlation [32].

In each encoder, code sequence generation and selection are provided by a serial combination of 2×2 switches and unit delays. The unit delays provide delays equal to the duration of a single chip and are made of either optical fibers or waveguides. In general, the encoder is basically constructed with a number of switching stages, each with a 2×2 switch and unit delay. Each 2×2 switch can be configured into two possible states (i.e., cross-bar or straight-through) according to its DC bias voltage, fed by the electronic address selector. The cross-bar state allows optical pulses to mix and to split inside a 2×2 switch, while the straight-through state allows optical pulses to pass through the switch without changes. At the input of the encoder, a narrow laser pulse is first split into two pulses by a passive coupler. One of the pulses is delayed and the amount of delay is accumulated as the pulse passes through straight-through-state 2×2 switches. After the proper amount of delay is obtained, the delayed pulse combines with the nondelayed one at a cross-bar-state 2×2 switch. At the same time, the two pulses then are split into four pulses (i.e., two pulses in each path) and the process repeats until the desired number of ones is generated.

Because of the serial structure, 2^n chip pulses are generated with n 2×2 switches in the cross-bar states and the rest in the straight-through states. Apparently, the total number of switches should depend on the sequence length N that is usually a large number. Actually, by carefully choosing the amount of delay (i.e., using nonunit delay) in each stage, the required number of switches can be reduced substantially.

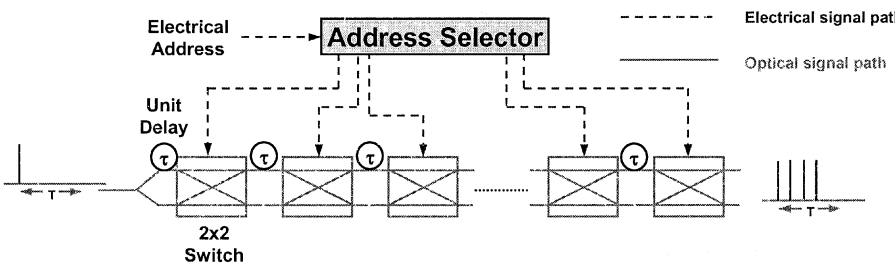

FIG. 13. All-serial encoder/decoder.

Serial-to-parallel encoder/decoders. For the all-parallel approach, a large number of delay lines and switches is needed, and for all-serial encoder, the number of switches is also very large. This cost will limit their application in practical systems. In order to implement the label encoder/decoder economically, we propose another approach called serial-to-parallel encoder/decoder.

The schematic diagram of serial-to-parallel encoder is shown in Fig. 14. The encoder includes three unit delay lines, four switches, a serial-to-parallel interleaver, and an optical combiner. At the input of the encoder, an optical pulse source is fed. The interleaver partitions the incoming code sequence into four subcode sequences via serial-to-parallel processing; for example, if the incoming code sequence is $C_0C_1C_2C_3C_4C_0C_1C_2C_3C_4C_0C_1\cdots$, after the interleaver we have the four subcode sequences $C_0C_4C_3\cdots$, $C_1C_0C_4\cdots$, $C_2C_1C_0\cdots$, $C_3C_2C_1\cdots$. These four subcode sequences are used to control the switches. When the pulse passes through the delay line path, four copies of the pulse are tapped out to pass through the switches. When the driving bit is ONE, the switch lets the pulse through; otherwise, the pulse is blocked. The optical combiner combines the outputs of the four switching paths to finish the coding processing.

Compared with the all-parallel and all-serial encoders, the serial-to-parallel encoder is more practicable. The advantages are: (1) it needs only three unit delay lines and is independent of the code length; (2) it needs only four switches, independent of the code length N_c; (3) it is suitable for OOC families of any format and any length; (4) it relaxes the requirement for the switching rate by four times; and (5) it can be integrated with the optoelectronics technology. Of course, the encoder requires more synchronization among the four subsequences.

Comparison of the three kinds of encoders/decoders. In order to investigate the performance of these three kinds of encoders/decoders, we compare five parameters under the same conditions. The five parameters are (1) the number of switches, (2) the number of unit delay lines, (3) switching time, (4) power loss, and (5) encoded extinction ratio.

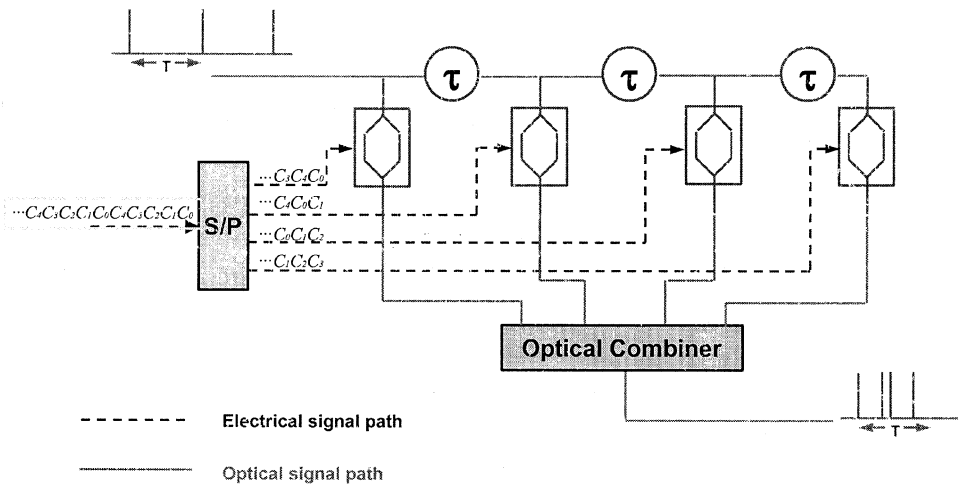

FIG. 14. Serial-to-parallel encoder/decoder.

TABLE 1
Comparison of three encoder/decoder approaches. N_c is the code length, n is the parameter of 2^n code, T_0 is the chip width, P is the code weight, r_0 is the original extinction ratio, and a is the degraded factor by a switch

	All-parallel encoder	All-serial encoder	Serial-to-parallel encoder
Switch number	N_c	$O(N_c)$	4
No. of units delay line	$N_c^2/2$	$O(N_c)$	3
Switch rate	T_0	T_0	$4T_0$
Power loss	$10\log_{10} N_c$	$30(n+2)$	$30(\log_{2^{P+2}})$
Extinction ratio	$r_0^* a$	$r_0^* a^n$	$r_0^* a$

In Table 1, the three kinds of encoders are compared with respect to these five parameters, where N_c is the code length, n is the parameter of 2^n code, T_0 is the chip width, P is the code weight, r_0 is the original extinction ratio and a is the degraded factor by a switch. From the comparison, it is seen that the serial-to-parallel encoder approach outperforms both the all-parallel encoder and the all-serial encoder in implementation practicability.

B. Time-gate-intensity-threshold (TGIT) device. As with all optical networks, chromatic dispersion [33] is one of the key issues that corrupts the transmitted signal and limits the cascadability of the networks. It is even worse in OCDMA systems, where the chip rate is generally L times the effective data rate due to the spreading. Another critical issue for an OCDM label network is the multiaccess Interference (MAI) and sidelobes of the autocorrelation of the code, which can also degrade the system performance. Therefore, schemes to alleviate dispersion effect and suppress sidelobes are required.

In order to combat chromatic dispersion and suppress sidelobes, a device called time-gating-intensity-thresholding (TGIT) device is proposed. It is a two-stage device, the first stage is dedicated for time gating, and the second stage is dedicated for intensity thresholding. In Fig. 15, a schematic diagram of TGIT is shown with its operational principle.

As shown in Fig. 15, the time-gating section is actually a pulse-sampling device that selects the auto correlation central spike. Thus, it can be used to improve the pattern recognition contrast for the distorted waveform, making the transmission more immune to the effects of dispersion. Time-gating is an all-optical process, which essentially operates as a time-domain demultiplexer. Therefore, the time-gating section also suppresses any sidelobes originating from the autocorrelation of the optical code, and reduces the effect of any interfering channels outside the time frame of the main autocorrelation peak.

For our design, we need an optical pulse as the pulse source of the final encoding stage when the data bit is ONE, and this optical pulse should not come out for a data bit ZERO. Thus, in the TGIT device, the second section performs optical intensity threshold processing. As shown in Figs. 15b and 15c, when the received

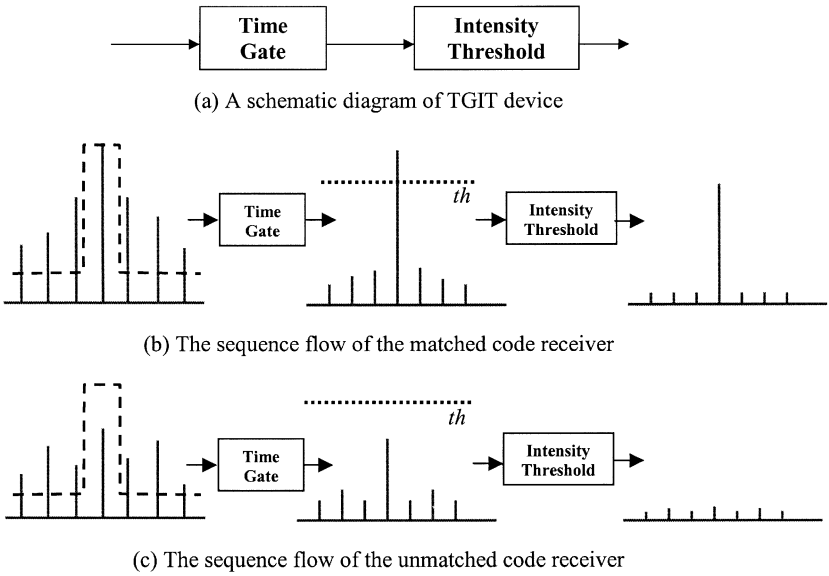

(a) A schematic diagram of TGIT device

(b) The sequence flow of the matched code receiver

(c) The sequence flow of the unmatched code receiver

FIG. 15. Schematic diagram of the TGIT device with its operational principle.

data bit is a ONE, the demultiplexed central peak is over the threshold value. Then after the threshold device, an optical pulse can be generated for the final encoding stage. On the other case, when the received data bit is ZERO, the demultiplexed central peak is below the threshold value, and then no optical pulse will come out after the threshold device.

With a two-stage TGIT device, we can combat the detrimental effects of chromatic dispersion and suppress the sidelobes of the autocorrelation and the cross-correlations [34]. Moreover, with a two-stage architecture, code conversion and wavelength conversion become independent. This provides more flexibility to the proposed networks. This issue will be discussed in the implementation of TGIT device.

Both the time-gating section and the intensity-thresholding section of TGIT device can be implemented with an optical time-domain multiplexer. Currently, there are mainly four candidates for optical time-domain multiplexer: (1) nonlinear optical loop mirror (NOLM) [35], (2) terahertz optical asymmetric demultiplexer (TOAD) [36], (3) ultrafast nonlinear interferometer (UNI) [37], and (4) Mach–Zehnder interferometer (MZI) [38]. To implement the TGIT device, we can choose according to the data/chip rate, cost, and flexibility. In the following, as an example, the architecture, the operational principles, and the features of a two-MZI-based TGIT device are investigated.

Figure 16 shows a TGIT device architect with two MZIs. The first MZI works as the time-gating device; the second MZI works as the intensity-thresholding device. The output of the decoder is fed into the time-gating device. The MZI is driven with a mode-locked laser (MLL) operating at an intermediate wavelength λ_{int}. After the bandpass filter (BPF), the central peak of the decoder output is demultiplexed and converted to wavelength λ_{int}, and the sidelobes are much suppressed at the same time. In the second stage-threshold device, the demultiplexed central peak is used

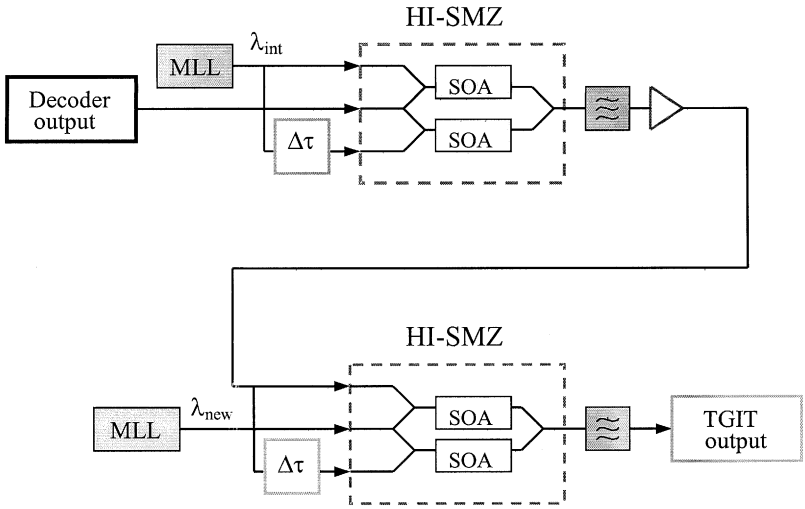

FIG. 16. The architecture of a two-stage time-gating-intensity-thresholding (TGIT) device based on two Mach–Zehnder interferometers. SOA: semiconductor optical amplifier; MLL: mode-locked laser; HI-SMZ: hybrid-integrated symmetric Mach–Zehnder; λ_{int}: intermediate wavelength; λ_{new}: new wavelength.

as the control pulse of the MZI device, and another MLL (wavelength λ_{new}) is used as the new pulse source. Then after the second BPF, the demultiplexed pulse is enhanced or suppressed according to the comparison between the intensity and the threshold value. Meanwhile, the final output is converted to a new wavelength. If we do not need wavelength conversion in the design, we can set the new wavelength λ_{new} equal to the original wavelength, otherwise, we can choose the new wavelength as the desired wavelength determined by the control plane. Therefore, code conversion and wavelength conversion can be realized independently. To reduce the cost, some MLLs, for instance MLLs at λ_{int}, can be shared by multiple TGIT devices in practical implementation.

IV. FUNDAMENTAL LIMITATIONS ON OOC/WAVELENGTH LABELED OMPLS NETWORK

1. Limitation on Label Switching Capacity

The limitation on label switching capacity arises when MAI exceeds the threshold of the gate device, generating a "ghost" pulse or an encoding error in the code-regeneration stage. The rate at which this error occurs is termed the code conversion error rate (CCER). To derive the CCER, we assume:

1. There are M co-propagating code channels that employ M quasi-orthogonal codes in N wavelengths;
2. All channels have identical average input powers at each decoder element;
3. Every channel has an identical bit rate; and
4. The path length difference in the decoder is longer than the sources' coherence length.

From [12], the CCER was derived as

$$PE_{CCER}(Th) = \frac{1}{4}\left[\operatorname{erfc}\left(\frac{Th-(M-1)\mu}{\sqrt{2}\sigma_Z}\right) + \operatorname{erfc}\left(\frac{W+(M-1)\mu-Th}{\sqrt{2}\sigma_Z}\right)\right]. \quad (1)$$

where Th is the threshold value of the gate device, μ and σ_z are the mean and variance of the individual interference signal $I_n^{(1)}$, and erfc$(*)$ is the complementary error function, defined as

$$\operatorname{erfc}(x) = \frac{2}{\sqrt{\pi}}\int_x^{\infty} e^{-t^2}dt. \quad (2)$$

To avoid lengthy calculations of all possible cross-correlation functions of a certain OOC set, the CCER bounds under two extreme conditions are analyzed. One is the chip synchronous case corresponding to an upper bound, and the other is the chip asynchronous case with worst-case scenario corresponding to a lower bound [39, 40]:

$$PE_{CCER}^{UP}(Th) = \frac{1}{4}\operatorname{erfc}\left(\frac{Th-(M-1)\frac{W^2}{2L}}{\sqrt{2\left[\sigma_T^2+(M-1)\frac{W^2}{2L}\left(1-\frac{W^2}{2L}\right)\right]}}\right) + \frac{1}{4}\operatorname{erfc}\left(\frac{W+(M-1)\frac{W^2}{2L}-Th}{\sqrt{2\left[\sigma_T^2+(M-1)\frac{W^2}{2L}\left(1-\frac{W^2}{2L}\right)\right]}}\right) \quad (3)$$

$$PE_{CCER}^{LOW}(Th) = \frac{1}{4}\operatorname{erfc}\left(\frac{Th-(M-1)\frac{W^2}{2L}}{\sqrt{2\left[\sigma_T^2+(M-1)\frac{W^2}{L}\left(\frac{1}{3}-\frac{W^2}{4L}\right)\right]}}\right) + \frac{1}{4}\operatorname{erfc}\left(\frac{W+(M-1)\frac{W^2}{2L}-Th}{\sqrt{2\left[\sigma_T^2+(M-1)\frac{W^2}{L}\left(\frac{1}{3}-\frac{W^2}{4L}\right)\right]}}\right). \quad (4)$$

W and L are the code weight and code length. Using Eq. (3) and Eq. (4), the CCER's upper and lower bounds are plotted with respect to the threshold value in Fig. 17, showing similar trends for both the upper bound and the lower bound. The combination of the MAI and the quantum noise yields a CCER floor for the proposed code converter. This is shown in Fig. 18, where the CCER floor (upper bound) is plotted against the number of code label channels to illustrate the effects of MAI on the label switching capacity of each switch fabric. For code weights of 5 or 10 and code lengths of 800 or 1500, the switch fabric can support up to 12 code channels per wavelength with an acceptable CCER floor of 10^{-9}. If there are k wavelengths available in the OMPLS network, the total number of label will be $12k$. According to IETF RFC3032 (Jan. 2001), 20 bits are to be allocated for the address field of the label in MPLS. However, it is only applicable to the first approach, the (IP + MPLS)/optical layer mentioned in Section I of this work. While

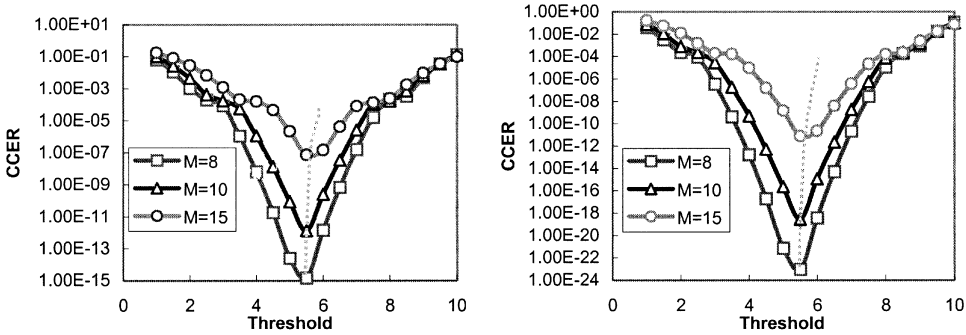

FIG. 17. The code conversion error rate (CCER) against the threshold value: (a) upper bound and (b) lower bound. $W = 10$, $L = 1000$, $\sigma_n = 0.01$, and $M = 8, 10$, and 15 as shown.

for the OMPLS approach, the label has only local meaning, which is not subject to the IETF RFC3032. Therefore, the number $12k$ can meet the label number requirements for a reasonable MAN/WAN scale.

Our proposed core router for the optical MPLS network can be of multiple fibers as shown in Fig. 19. Under this scenario, the derivation of the CCER floor is the same as the above.

2. Limitation on Network Throughput Due to LSR Reconfigurability

In an OMPLS network, the optical bandwidth is assigned into various traffic trunks indicated by different optical labels. When a new session is set up, the traffic is mapped onto an optical label at the ingress router, and forwarded by the intermediate routers through label swapping until the optical label is removed at the egress router. As described in the draft of the Internet engineering task force (IETF) [41], there are four cases in which the size of the label set will be limited. The first case

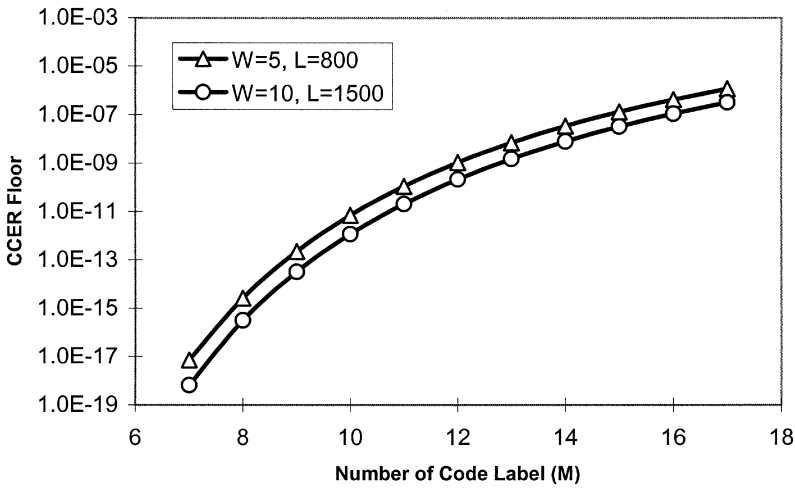

FIG. 18. The CCER floor of the upper bound versus the number of code channels per wavelength. The traces converge to 0.5.

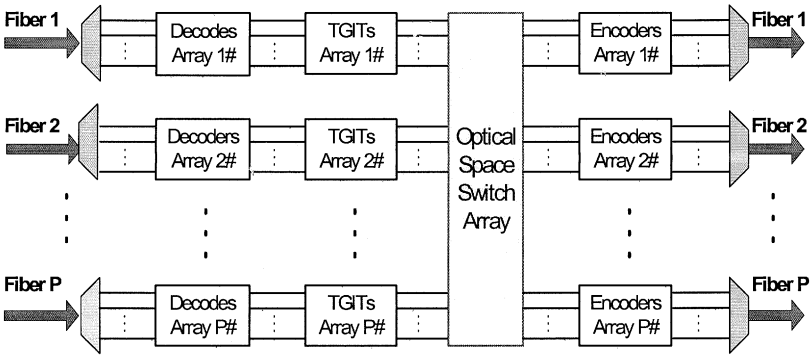

FIG. 19. The schematic diagram of the multifiber code-based OMPLS router.

is that the end equipment is only capable of transmitting and receiving on a small specific set of wavelengths/bands. The second case is that there are some intermediate nodes that have no wavelength conversion capability and require the same wavelength used end-to-end over consecutive hops, or even the entire path. The third case is that it is desirable to limit the amount of wavelength conversion being performed to reduce cost and possible distortion on the optical signals. The last case is that the two ends of a link support different sets of wavelengths. These four scenarios result in different capacities of each link and affect the performance of transport networks.

Our proposed optical routing network is not exempted from these kinds of physical limitations. The forwarding function is performed by optical code and wavelength conversion. As mentioned above, these physical limitations would result in different capacities of the links and correspondingly lead to the mismatch of the code/wavelength label sets along the links. One of the cases is the different conversion capability of the core routers that can limit the available labels used on the optical LSP (label switched path). It will limit the network throughput, and blocking probability will be degraded. In this section, we focus on the case where there are routers in the network that cannot perform wavelength conversion, thus inducing some constrains to the blocking performance of the networks.

A. LSR Reconfigurability-Conversion Capability. The physical layer infrastructure of the LSR can be viewed as an OXC that is able to perform optical conversion. Its conversion capability is determined by the construction of the TGIT device. As shown in Fig. 16, by tuning the working wavelength of the MLL in the second stage, the decoded signal can be converted to λ_{new}, which could be any of the wavelengths that are used in the next link. The wavelength-converted signal then is retransmitted after being re-encoded into a new optical label. Thus, the signal carried on a certain code/wavelength label (c, λ) is mapped optically onto another available code/wavelength labeled (c', λ'), with $c, c' \in [1, M]$ and $\lambda, \lambda' \in [1, N]$, at an OMPLS core router that has full-conversion capability.

By using fixed wavelength MLLs, the router can be configured with only code conversion, which is called CR. For the CR, the input optical signal on the label (c, λ) can be converted to the label (c', λ), with the wavelength unchanged. It is

obvious that CRs cost less, but will limit the optical labels used for establishing the optical LSP.

In the following, analytical results of blocking probabilities of LSP under three different scenarios of conversion capability are derived and the performance gain under different conversion capability is analyzed and shown graphically.

B. Blocking Probability Derivation. In this part, we will investigate the blocking performance of the OMPLS networks with explicit routing. The OMPLS networks deploy the LSRs with different conversion capabilities.

For a conventional wavelength routing network, Barry's formula provides equations to study the qualitative behavior of the networks by making a simplistic traffic assumption [42]. In Barry's formula, a path without wavelength conversion is decomposed into fixed-wavelength lightpaths whose blocking probabilities are independent. The end-to-end blocking probability of the path is obtained by calculating the blocking probability of each lightpath.

For a path that is equipped with wavelength conversion at each node, the blocking in each hop is independent. Again, by taking apart the path into independent segments, the blocking probability of a path with wavelength conversion can be derived by calculating the blocking of each segment.

In the following, we will extend Barry's analysis to a two-dimensional problem in order to investigated blocking performance of our proposed code/wavelength labeled OMPLS network. We consider the single-fibered network with N wavelengths per fiber and M codes per wavelength. There are all together $N \times M$ code/wavelength channels in a link, and each channel is assumed to have a uniform load of ρ.

LSP with CRs only. Since the routers along the established optical LSP have no ability of wavelength conversion but only code conversion, under this scenario, the establishment of the LSP should comply with the fixed wavelength constraint. Here, we regard all the code channels on a wavelength of one hop as a trunk. A certain trunk n is said busy if all the code channels in it are occupied, otherwise it is free. We define the successive trunk sequence between the source and destination nodes as a trunk path. The trunk path is said to be successful if the end-to-end connections can be set up within it; otherwise it is regarded as blocked. It is clear that, between the source and destination nodes, the number of fixed wavelength trunk paths are N, which equals the number of wavelengths. These N wavelength trunk paths are independent. On each trunk there are M code channels and M is the code number per wavelength. Therefore, the blocking probability of an H-hop LSP could be derived as

$$\begin{aligned} P_{BC}(H, N, M) &= P\{\text{all } N \text{ fixed-wavelength trunk path are blocked}\} \\ &= \prod_{n=1}^{N} P\{ \text{ the trunk path } n \text{ is blocked}\}. \end{aligned}$$

Note that the blocking probability of each trunk path n is equal to the blocking probability of the conventional wavelength routing network with wavelength converters as derived in [42]. Therefore, the blocking probability of the LSP with only

CRs can be expressed as

$$P_{BC} = (H, N, M) = \prod_{n=1}^{N}(1 - (1 - \rho^M)^H) = (1 - (1 - \rho^M)^H)^N, \quad (5)$$

where ρ is the link load. Thus we show that for this case, the original two-dimensional (code/wavelength) routing problem can be decomposed into a one-dimensional routing problem.

LSP with FRs only. In the case that all the routers are equipped with full conversion capability, there are $N \times M$ independent channels with uniform link load ρ for each hop. In this case, we can regard the two-dimensional channels (N wavelength and M code) as one-dimensional channels with channel number $N \times M$. Referring to the derivation from [42], the blocking probability can be approximated as:

$$P_{BF}(H, N, M) = 1 - (1 - \rho^{N \times M})^H, \quad (6)$$

LSP with FRs and CRs. As discussed above, since the FRs are much more costly than CRs, it is worthwhile to investigate how to sparsely place the FRs in the network and find a balance between cost and performance.

The ratio of the number of FRs to the total number of intermediate routers along the LSP is defined as the placement density q. In the following, we will see how the placement density affects the blocking performance of the LSP.

Referring to [43], the uniform placement is a proven optimal scheme in a conventional wavelength routing network with sparsely placed wavelength converters. Therefore, we assume a uniform placement of the FRs along the optical LSP and CRs at the remaining nodes. In this case, the FRs will separate the LSP into K subpaths. Each sub-LSP is equivalent to the LSP in case (1) that has CRs only. The blocking probability of the kth sub-LSP can be derived from Eq. (5):

$$P\{S^k = 0\} = (1 - (1 - \rho^M)^l)^N.$$

And the blocking probability of the LSP under the scenario of uniform placement is

$$P_{BCF}(H, N, M, K) = 1 - \prod_{k=1}^{K}(1 - P\{S^k = 0\}) = 1 - (1 - (1 - (1 - \rho^M)^l)^N)^K, \quad (7)$$

where K is the number of sub-LSP, l (equal to H/K) is the number of hops in a sub-LSP, and $P\{S^k = 0\}$ represents the blocking probability of the sub-LSP k. Note that the expression (7) is valid if H is an integer multiple of K; otherwise, the above equation is the lower bound of the actual blocking probability [43].

In an OMPLS core network, with the development of optical intelligence and the increase of heterogeneous services on the Internet, optical labels may be implemented on multiple orthogonal dimensions, such as time, wavelength, code, and subcarrier, to meet the demand on the optical channels. While that increases, the flexibility of the resource allocation, the difficulty of controlling and manage the network is also increased. We have derived the closed-form expressions for

blocking probability for three different OMPLS router configurations with optical code/wavelength labels. The results were obtained by decomposing the two-dimensional problem into a one-dimensional problem. This analysis method could be generalized into an iterative decomposition scheme for the multidimensional routing network. This can facilitate the analysis of the blocking probability and other performances of the network in closed-form expressions.

C. Numerical Results. Numerical results generated from the above equations are shown to illustrate the blocking probabilities and conversion gains under various converter configurations in our proposed OMPLS network with code/wavelength labels.

Figure 20 shows the blocking performance of 16-hop LSP with CRs only. At light link load and for wavelength number $N = 4$, the blocking performance of the LSP is improved significantly as the OOC number increases. Therefore, when a large set of OOC codes are employed, the code/wavelength-based OMPLS network performs well even when only CRs are equipped.

With the same number of total labels ($N \times M = 16$), Fig. 21 shows the blocking probability of a 16-hop LSP with CRs only. For the case $M = 1, N = 16$, this corresponds to the conventional wavelength routing network that has no wavelength conversion. The figure clearly shows that when the number of channels in the link is the same, the OMPLS networks with code/wavelength labels perform better when the code number increases. It is also found that the blocking performance is improved more significantly when the link loads are smaller. It is shown in Fig. 21 that when the link load is 0.2, compared with the case of $M = 1, N = 16$, there is a significant reduction in blocking probability (10^{-6}) when the code number is increased to 4.

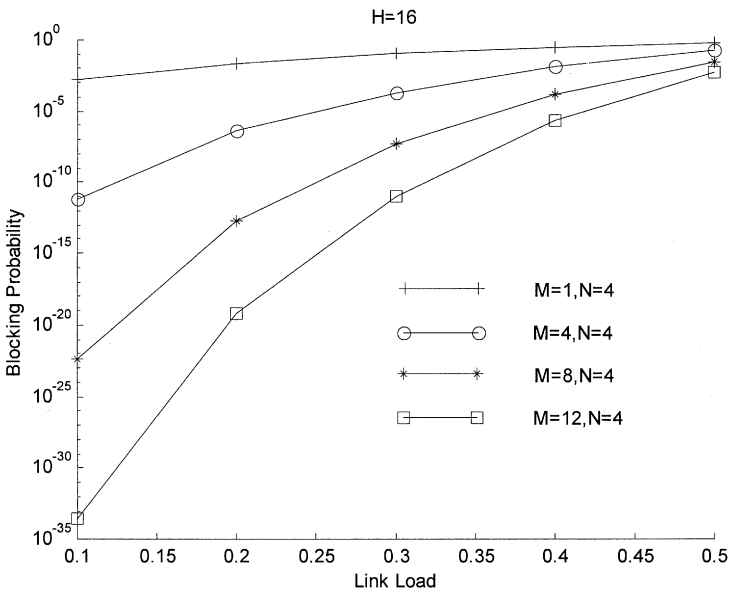

FIG. 20. The blocking probability versus the link load ρ with different numbers of OOC codes when only code conversion is performed.

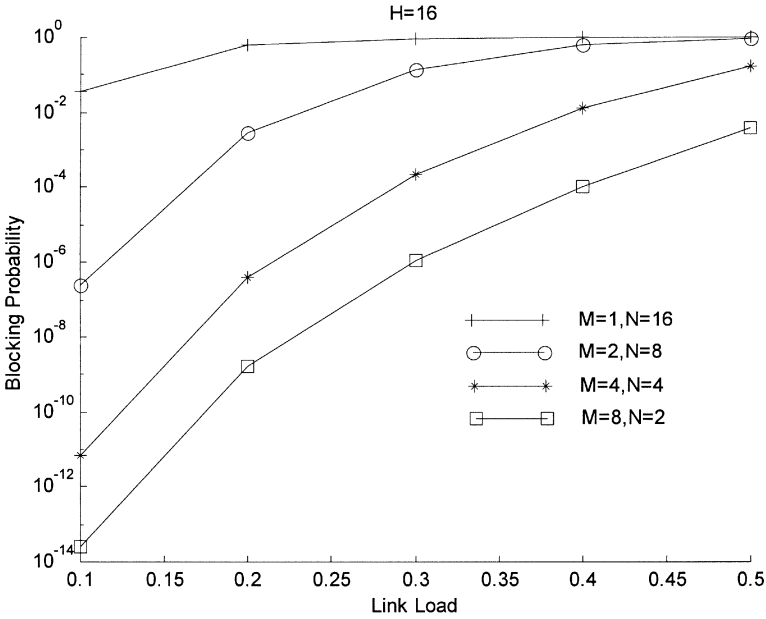

FIG. 21. The blocking probability versus link load ρ when only code conversion is performed at the router.

In Fig. 22, the conversion gain under different placement densities (q) is given. The conversion gain G is defined as $G = P_{BCF}(q)/P_{BCF}(0)$, where q equals $(K-1)/(H-1)$. When all the intermediate routers along the LSP are FRs, the placement density q is 1; when all the intermediate routers along the LSP are CRs, q is 0. Otherwise, the q value is between 0 and 1. In the simulation, the number of hops is

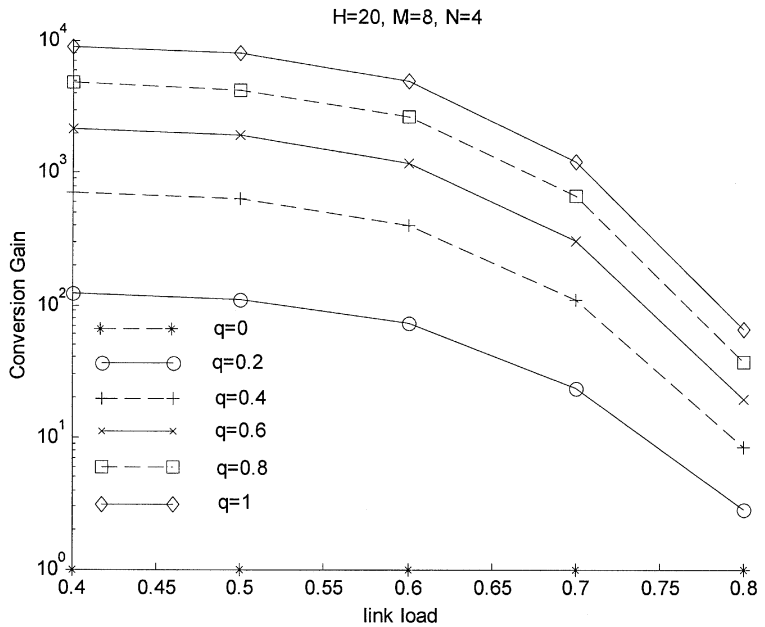

FIG. 22. The conversion gain G versus link load ρ at different placement density q.

20 and $M = 8, N = 4$. When link load is 0.4, even with a low placement density of $q = 0.2$, corresponding to uniformly placing of four FRs on the LSP and remaining nodes with CRs, the conversion gain is as high as 10^2. The conversion gain is 10^4 when $q = 1$.

V. CONCLUSION

In this paper, an optical MPLS network using code/wavelength as label is proposed. The architecture of core routers based on all-optical code/wavelength converter is illustrated. The fundamental limits on the scalability of the proposed core router, including the label capacity and network blocking probability, are investigated with closed-form solutions derived.

Due to the unipolar property of OOC, a code conversion error rate (CCER) floor results from the multiaccess interference (MAI) and the thermal noise. A closed-form CCER floor is shown. Accordingly, the label switching capacity, which is governed by the maximum number of code channels per wavelength, can be determined by the acceptable CCER floor.

By the mathematical analysis, closed-form results of the blocking probabilities for LSPs with two-dimensional labels under different conversion capabilities are derived. The performance gain under different conversion capability is analyzed and shown graphically. At the link load of 0.4, a conversion gain of 100 is achieved when l/5 of the CRs are replaced with FRs for a network with $M = 8$ and $N = 4$.

ACKNOWLEDGMENT

This project is supported in part by the Research Grant Council of Hong Kong, SAR, China (Project CUHK-4172/01E).

REFERENCES

[1] C. A. Brackett, "Dense wavelength division multiplexing networks: Principles and applications," *IEEE J. Select. Areas Commun.*, vo1. 8, 948 (1990).

[2] P. E. Green, Jr., L. A. Coldren, K. M. Johnson, J. G. Lewis, C. M. Miller, J. F. Morrison, R. Olshansky, R. Ramaswami, and E. H. Smithand, Jr., "All-optical packet-switched metropolitan-area network proposal," *IEEE/LEOS J. Lightwave Technol.*, vol. 11, no. 5, 754 (1993).

[3] D. Norte and A. E. Willner, "All-optical data format conversions and reconversions between the wavelength and time domains for dynamically reconfigurable WDM networks," *IEEE/LEOS J. Lightwave Technol.*, vol. 14, no. 6, 1170 (1996).

[4] K. Kitayama, "Code division multiplexing lightwave networks based upon optical code converter," *IEEE J. Selected Areas Commun.*, vol. 16, no. 7, 1309 (1998).

[5] D. J. Blumenthal, P. R. Prucnal, and J. R. Sauer, "Photonic packet switches: Architectures and experimental implementations," *Proc. IEEE*, vol. 82, no. 11, 1650 (1994).

[6] A. Jourdan *et al.*, "The perspective of optical packet switching in IP-dominant backbone and metropolitan networks," *IEEE Commun. Mag.*, vol. 39, no. 3, 136 (2001).

[7] Gee-Kung Chang *et al.*, "Low latency packet forwarding in IP over WDM networks using optical label switching techniques," presented at OFC'99, San Diego, Paper MB1.

[8] A. Viswanathan *et al.*, "Evolution of multiprotocol label switching," *IEEE Commun. Mag.*, vol. 36, 165 (1998).

[9] A. Banerjee *et al.*, "Generalized multiprotocol label switching: An overview of routing and management enhancements," *IEEE Commun. Mag.*, vol. 39, no. 1, 144 (2001).

[10] K. Kitayama and N. Wada, "Photonic IP routing," *IEEE Photon. Technol. Lett.*, vol. 11, 1689 (1999).

[11] Yong-gang Wen, Yu Zhang, Lian-kuan Chen, and Frank Tong, "An optical routing network based on code/wavelength label switching technology. I. Architecture," submitted for publication.

[12] Yong-gang Wen, Yu Zhang, Lian-kuan Chen, and Frank Tong, "An optical routing network based on code/wavelength label switching technology. II. Scalability," submitted for publication.

[13] D. J. Blumenthal *et al.*, "All-optical label swapping networks and technologies," *IEEE/LEOS J. Lightwave Technol.*, vol. 18, no. 12, 2058 (2000).

[14] C. A. Bracket, "Dense wavelength division multiplexing networks: Principles and applications," *IEEE J. Selected Areas Commun.*, vol. 8, no. 8, 948 (1990).

[15] P. Toliver, K.-L. Deng, I. Glesk, and P. R. Prucnal, "Simultaneous optical compression and decompression of 100-Gb/s OTDM packets using a single bidirectional optical delay line lattice," *IEEE Photon. Technol. Lett.*, vol. 11, 1183 (1999).

[16] A. Viswanathan, N. Felfman, Z. Wang, and R. Callon, "Evolution of multiprotocol label switching," *IEEE Commun. Mag.*, vol. 36, 165 (1998).

[17] T. Fjelde, A. Kloch, and D. Wolfson, "Novel scheme for efficient label-swapping using simple XOR gate," in *Proceedings of ECOC'2000*, vol. 4, pp. 63–64, 2000.

[18] N. Wada, H. Harai, W. Chujo, and F. Kubota, "Photonic packet switching based on multi-wavelength label switching using fiber Bragg gratings," presented at ECOC'2000, paper P10.4.6, Munich, Germany, Sept. 3–7, 2000.

[19] A. Carena, M. D. Vaughn, R. Gagudino, M. Shell, and D. J. Blumenthal, "OPERA: An optical packet experimental routing architecture with label swapping capability," *IEEE/LEOS J. Lightwave Technol.*, vol. 16, no. 12, 2135 (1998).

[20] S. J. B. Yoo, J. L. Hyuek, Srikanth Vaidianathan, K. Okamoto, and K. Shin, "Optical-label switching and routing by rapidly tunable wavelength conversion and uniform loss cyclic frequency array-waveguide grating," in *Proceedings of OFC'2001*, paper WDD49.

[21] Y. M. Lin, W. I. Way, and G. K. Chang, "A novel optical label swapping technique using erasable optical single-sideband subcarrier label," *IEEE Photon. Technol. Lett.*, vol. 12, no. 8, (2000).

[22] N. Wada and K. Kitayama, "10 Gb/s optical code division multiplexing using 8-chip optical bipolar code and coherent detection," *IEEE/LOES J. Lightwave Technol.*, vol. 17, 1758 (1999).

[23] K. Kitayama *et al.*, "Architectural considerations for photonic IP router based upon optical code correlation," *IEEE/LEOS J. Lightwave Technol.*, vol. 18, no. 12, 1834 (2000).

[24] Y. G. Wen, L. K. Chen, K. P. Ho, and F. Tong, "An all-optical code converter scheme for OCDM routing networks," presented at ECOC'2000, paper P4.5, Munich, Sept. 3–7, 2000.

[25] Y. G. Wen, L. K. Chen, and F. Tong, "Fundamental Limitation and Optimization on Optical Code Conversion for WDM Packet Switching Networks," in *Proceedings of OFC'2001*, paper TUv-5.

[26] H. Sotobayashi *et al.*, "Broadcast-and-select OCDM/WDM network using 10Gbit/s spectrum-sliced supercontinuum BPSK pulse code sequences," *IEE Electron. Lett.*, vol. 35, no. 22, 1966 (1999).

[27] Chih-Hong Eyoh *et al.*, "Architecture of ATM transit switching using optical CDMA technique," presented at International Conference on Information, Communications and Signal Processing, ICICS'97, pp. 873–877, Singapore, Sept. 9–12, 1997.

[28] F. R. K. Chung *et al.*, "Optical orthogonal codes: Design, analysis and applications," *IEEE Trans. Inform. Theory*, vol. IT-35, 595 (1989).

[29] A. S. Holmes *et al.*, "All-optical CDMA using quasi prime codes," *IEEE/LEOS J. Lightwave Technol.*, vol. 10, 279 (1992).

[30] W. C. Kwong and P. R. Prucnal, "Programmable ultrafast all-optical code-division multiple access networks," in *Proceedings of OFC'92*, p. 134, San Jose, CA, February 1992.

[31] P. R. Prucnal *et al.*, "Spread spectrum fiber-optic local area network using optical processing," *IEEE/LOES J. Lightwave Technol.*, vol. LT-4, 547 (1986).

[32] W. C. Kwong *et al.*, "Demonstration of a programmable ultrafast all-optical code-division multiple access network," in *Proceedings of CLEO'92*, pp. 44–45, Anaheim, CA, May 1992.

[33] P. Ohlen, L. Thylen, and E. Berglind, "Dispersion limits in 10Gb/s standard fiber systems using nonlinear optoelectronics repeaters," *IEEE Photon. Technol. Lett.*, vol. 9, no. 8, 1155 (1997).

[34] N. Wada, H. Sotobayashi, and K. Kitayama, "Error-free 100 km transmission at 10Gb/s in optical code division multiplexing system using BPSK picosecond-pulse code sequence with novel time-gating detection," *Electron. Lett.*, vol. 35, 833 (1999).

[35] Ding Wang *et al.*, "Nonlinear optical loop mirror based on standard communication fiber," *IEEE/LEOS J. Lightwave Technol.*, vol. 15, no. 4, 642 (1997).

[36] J. P. Prucnal *et al.*, "A terahertz optical asymmetric demultiplexer (TOAD)," *IEEE Photon. Technol. Lett.*, vol. 5, no. 7, 787 (1993).

[37] N. S. Patel, K. A. Rauschenbach, and K. L. Hall, "40-Gb/s demultiplexing using an ultrafast nonlinear interferometer (UNI)," *IEEE Photon. Technol. Lett.*, vol. 8, no. 12, 1695 (1996).

[38] S. Nakamura *et al.*, "Error-free all-optical data pulse regeneration at 84 Gbps and wavelength conversion with symmetric Mach–Zehnder all-optical switches," in *Proceedings of OAA'2000*, PDP4.

[39] J. A. Salehi, "Code division multiple-access techniques in optical fiber networks. I. Fundamental principles," *IEEE Trans. on Commun.*, vol. 37, no. 8, 824 (1989).

[40] J. A. Salehi and C. A. Brackett, "Code division multiple-access techniques in optical fiber networks. II. Systems performance analysis," *IEEE Trans. Commun.*, vol. 37, no. 8, 834 (1989).

[41] P. Ashwood-Smith *et al.*, "Generalized MPLS—Signaling functional description," Internet-draft, http://www.ietf.org/internet-drafts/draft-ietf-mpls-generalized-signaling-07.txt, Nov. 2001.

[42] R. A. Barry and P. A. Humblet, "Model of blocking probability in all-optical network with and without wavelength changers," *IEEE J. Select. Areas Commun.*, vol. 14, 858 (1996).

[43] S. Subramaniam, M. Azizoglu, and A. K. Somani, "On optimal converter placement in wavelength-routed networks," *IEEE/ACM Trans. Networking*, vol. 7, no. 5 (1999).